

# MobileH2R: Learning Generalizable Human to Mobile Robot Handover Exclusively from Scalable and Diverse Synthetic Data

Zifan Wang<sup>\*1,2</sup> Ziqing Chen<sup>\*1,2</sup> Junyu Chen<sup>\*1</sup> Jilong Wang<sup>2,3</sup> Yuxin Yang<sup>2</sup>  
Yunze Liu<sup>1,5</sup> Xueyi Liu<sup>1,5</sup> He Wang<sup>2,3</sup> Li Yi<sup>†1,4,5</sup>

<sup>1</sup>Tsinghua University <sup>2</sup>Galbot <sup>3</sup>Peking University

<sup>4</sup>Shanghai Artificial Intelligence Laboratory <sup>5</sup>Shanghai Qi Zhi Institute

<https://MobileH2R.github.io>

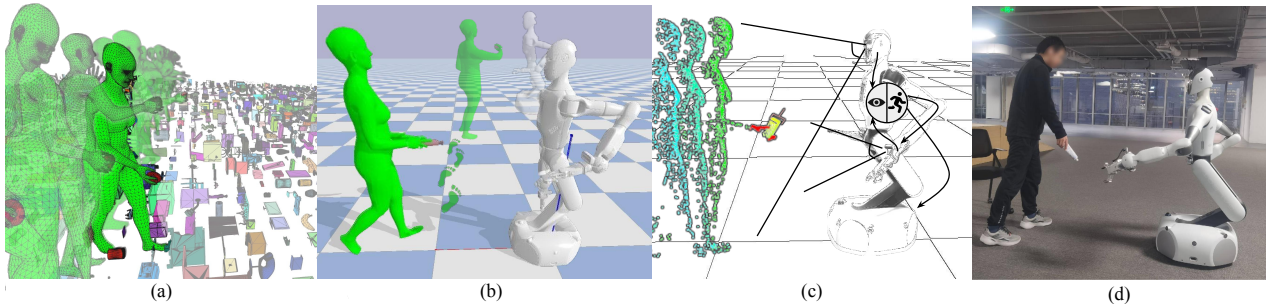


Figure 1. **The overview of MobileH2R.** We propose a framework for generalizable human-to-mobile-robot handover, including a scalable pipeline for diverse full-body human motion synthesis (a), an automatic method for producing safe, imitation-friendly demonstrations (b), an efficient 4D imitation learning approach to learn coordinated base-arm actions (c), and successful sim2real transfer (d).

## Abstract

*This paper introduces MobileH2R, a framework for learning generalizable vision-based human-to-mobile-robot (H2MR) handover skills. Unlike traditional fixed-base handovers, this task requires a mobile robot to reliably receive objects in a large workspace enabled by its mobility. Our key insight is that generalizable handover skills can be developed in simulators using high-quality synthetic data, without the need for real-world demonstrations. To achieve this, we propose a scalable pipeline for generating diverse synthetic full-body human motion data, an automated method for creating safe and imitation-friendly demonstrations, and an efficient 4D imitation learning method for distilling large-scale demonstrations into closed-loop policies with base-arm coordination. Experimental evaluations in both simulators and the real world show significant improvements (at least +15% success rate) over baseline methods in all cases. Experiments also validate that large-scale and diverse synthetic data greatly enhances robot learning, highlighting our scalable framework.*

## 1. Introduction

The embodied AI research community has long been motivated by the goal of enabling robots to interact and collaborate naturally with humans. A key challenge is the development of human-to-mobile-robot (H2MR) handover, which requires robots to reliably receive objects handed over by humans across a large, reachable space enabled by their mobility. This capability is crucial in diverse settings such as healthcare assistants and industrial assembly lines, where mobile robots must seamlessly interpret and respond to human actions to perform tasks efficiently and safely.

However, learning generalizable interaction skills between humans and robots presents several unique challenges. Unlike human-free robot manipulation, human-to-robot (H2R) handover remains difficult to scale effectively. Real-world H2R training introduces significant safety risks and costs, making direct training with humans inherently non-scalable. Simulated environments have been proposed as a solution to circumvent these challenges, but creating large-scale, realistic human motion and object assets is itself a demanding task. The first H2R simulation Handover-Sim [3] uses mocap data DexYCB [2] in simulation realistic assets in simulation, but with only 1,000 sequences, it lacks

the complexity needed to reflect real-world interactions.

The challenges intensify in H2MR handover, where robots must interpret full-body human actions while managing mobility and navigation complexities. Traditional approaches break down handover into subtasks like grasp estimation and trajectory planning [20, 53], which limits holistic environmental modeling and hinders generalizability. Recent methods, such as GenH2R [49], advance with end-to-end frameworks that scale through synthetic assets, but these often constrain interactions to fixed-base robotic arms or only capture partial human motions, like hand gestures, without full-body movement modeling.

In this work, we aim to achieve generalizable H2MR handover by addressing these challenges. Our key insight is that generalizable handover skills can be developed in simulators without the need for real-world demonstrations, as long as high-quality synthetic data—comprising human motion assets, object assets, and robot demonstrations—is utilized. We introduce a comprehensive solution that scales both assets and demonstrations, enabling effective closed-loop visuomotor policy learning through imitation.

To scale up synthetic and diverse full-body human motion data, we introduce an automatic pipeline emphasizing both diversity and fidelity. Existing datasets like AMASS [30], and MotionX [26] lack task-specific specialization as well as interactive behaviors for complex HRI tasks like handover. Therefore, We propose a two-stage pipeline for full-body handover motion synthesis. By leveraging some generic motion synthesis algorithms [23], we generate a wide range of realistic full-body motions, while a task-specific synthesis method creates diverse hand and arm movements tailored for handovers. Furthermore, we design an interactive human agent to respond to the robot’s proximity. Our synthetic dataset includes over 100K interactive handover scenes, scalable for task-specific HRI training.

To ensure safe interaction, we opt to learn interaction policies through imitation rather than reinforcement learning. Inspired by GenH2R [49], we explore motion planning methods for demonstration generation. In terms of safety, we optimize the planner to ensure that the planned trajectories avoid collisions with the human body and prevent entering the human’s blind side. To further facilitate the imitation from the demonstrations, we also ensure that the vision sequence paired with the planned trajectory provides clear and informative object state estimates. Since object states are strongly correlated with the robot’s actions, this also strengthens the connection between the vision signal and the robot’s actions, making imitation learning more effective. To implement all these requirements, we define several losses in the motion planning process to ensure the generation of high-quality demonstrations.

Finally, to distill these demonstrations into a visuomotor policy, we employ a 4D imitation learning approach that

incorporates both human and object vision inputs, along with coordinated base-arm action outputs. Unlike previous works [5, 49] that focus solely on hand-object point clouds, our approach also includes the human body as input. To address scale differences between body and object point clouds, we apply set abstraction layers with varied sampling radii. The resulting features are merged into a global representation and decoded using an MLP to generate coordinated base-arm movements, which are essential for controlling a mobile robot.

We evaluate our learned policy in both simulators and the real world. Notably, without relying on human mocap assets or real-world robot demonstrations, our method outperforms baselines in all settings, achieving at least **+15%** improvement in success rate. Our experiments demonstrate that scaling up demonstration size and enriching scene variety significantly enhances policy generalizability. Furthermore, the automatically generated scalable demonstrations improve safety and accuracy, reducing collisions by about 1/3 and increasing success rates by 11.6% while facilitating skill transfer to real mobile robot systems.

In summary, the key contribution of this paper is a novel, automated framework that scales learning for H2MR handover, consisting of three main components: i) a scalable pipeline for generating diverse synthetic full-body human motion data for the handover task, ii) an automatic pipeline that generates safe, imitation-friendly demonstrations for vision-based closed-loop control, and iii) a 4D imitation learning method for distilling large-scale demonstrations into closed-loop policies with base-arm coordination.

## 2. Related Work

### 2.1. Human-to-Robot Handovers

Recent advancements in human-robot handovers [6, 11, 49] have been fueled by the growing interest in human-robot interaction [33, 35] and the availability of large datasets [2, 9, 10, 13, 28, 54] capturing hand-object interactions. Grasping and dynamic motion planning [16, 53, 56] are potential solutions but often face limitations in motion flexibility and large-scale datasets. HandoverSim [3] and GenH2R-Sim [49] provide physics-based environments and benchmarks for H2R handovers. By leveraging mocap data or large synthetic datasets, these platforms enable training learning-based policies [4, 5, 49]. However, these methods focus on fixed-base H2R handovers and do not consider large workspaces. [20] attempts to decouple object pose estimation from planning, but it lacks scalability and does not model the environment comprehensively. In contrast, our proposed MobileH2R framework integrates human information, object data, and temporal context, solving the mobile handover task in an end-to-end manner. It incorporates scalable asset and demonstration generation processes,

along with an efficient imitation learning approach.

## 2.2. Mobile Robot Manipulation

Many real-world tasks, like human-to-mobile robot handovers, require coordinated body movements while manipulating objects [27, 45]. Many recent approaches separate navigation and manipulation using semantic controllers or motion planners [34, 50, 51]. [22, 24, 55] address long-horizon mobile manipulation tasks by leveraging predefined navigation and manipulation skills, typically through iterative or two-stage methods. However, these methods often overlook the need for coordinated arm and base actions. While some researchers [52] address human-free tasks with reinforcement learning for mobile manipulation, our focus on human interaction requires ensuring safety. Therefore, we choose imitation learning with safe demonstrations to learn coordinated arm-based actions for human safety.

## 2.3. Scaling up Demonstrations for Imitation

Imitation learning from large-scale demonstrations has emerged as a popular approach for robot learning. These demonstrations can be sourced from various channels, including real-world collections [36, 44], foundation models [19, 46, 48], non-robotics datasets [18], and generating through Task and Motion Planning (TAMP) [8, 17, 32]. GenH2R [49] has adapted the TAMP framework for dynamic handover scenarios in human-to-robot (H2R) interactions. In this work, we focus on a more challenging task: H2MR handover, where both the human and robot behaviors are more dynamic and diverse, necessitating the generation of safe and imitation-friendly demonstrations.

## 3. Method

For the generalizable human-to-mobile-robot handover task, we focus on a robot with a mobile base, controlling the movement of the base and the robotic arm. The robot is equipped with a head camera and a wrist camera for visual input. When the robot is positioned farther from the human, the head camera is mainly used for perception. As the robot moves closer, the wrist camera supplements the input to overcome occlusion caused by the arm. The model learns 6D control actions (3D translation and 3D rotation) for the robot gripper and 3D control actions (2D translation and 1D rotation) for the base, using segmented point cloud data of the human, hand, and object from both cameras. The framework is shown in Figure 2.

### 3.1. MobileH2R-Sim

There are two prime factors of large-scale synthetic human activities to resemble ground-truth distribution, i.e., diversity and fidelity (human-likeness). For task-specific human-robot interaction(HRI), like handover, two extra factors are

worth taking into consideration, i.e., specialization and interactivity. The human agent in human activities synthesis requires full awareness of the specific HRI task and interacts with the robot agent in the simulated environment.

Conventional methods for collecting human trajectories are often unsuitable for sophisticated HRI tasks. Existing large-scale datasets, such as Human3.6M [21], AMASS [30], and MotionX [26], lack task-specific focus. While motion capture or tracking techniques can be applied to specialized tasks, they are difficult to scale. The randomized trajectory generation approach, as implemented in GenH2R, can produce simple hand-object motions but cannot generate human-like motions. To address these challenges, we introduce MobileH2R-Sim, a simulation environment specializing in full-body motion synthesis for the H2MR handover task. The generation process is divided into two phases. During the pre-handover phase, our approach generates diverse, task-independent full-body movements. During the handover phase, we generate arm-only movements to smoothly transition from the previous actions and initiate the object transfer. Additionally, we incorporate an interactive design that responds to the robot’s actions, facilitating seamless transitions between the two phases, rather than relying on a static animation replay.

To generate diverse full-body movements during the pre-handover phase, we employ controllable generative models that distill a human motion prior from large-scale datasets. Specifically, we use Guided Motion Diffusion (GMD) [23] trained on the AMASS dataset, generating full-body actions based on prompts and offers significant advantages over other methods. Since our goal is not to generate physically feasible motions for simulation, but rather to provide diverse human motion for H2MR handover scenarios, this approach avoids the scalability limitations of real-world data.

For the arm-only movement during the handover phase, we adopt a task-specific local synthesis approach that introduces sufficient randomness. Unlike the full-body motion synthesis, this method focuses on the hand and arm movements involved in holding and transferring the object. The process consists of three stages: (1) identifying a feasible region in space for the handover and randomly sampling a point within it as the final handover position; (2) solving for the arm’s joint configuration at the final position using a kinematic optimizer that accounts for human joint constraints and movement habits; and (3) selecting an appropriate arm trajectory by calculating the difference between the initial and final positions, followed by interpolating intermediate frames to ensure smooth motion.

Another critical component is the interactive design, which allows for human responsiveness to the robot within the simulation to mimic the real world. When the robot is at a greater distance from the human, the human remains in the pre-handover phase, performing full-body movements

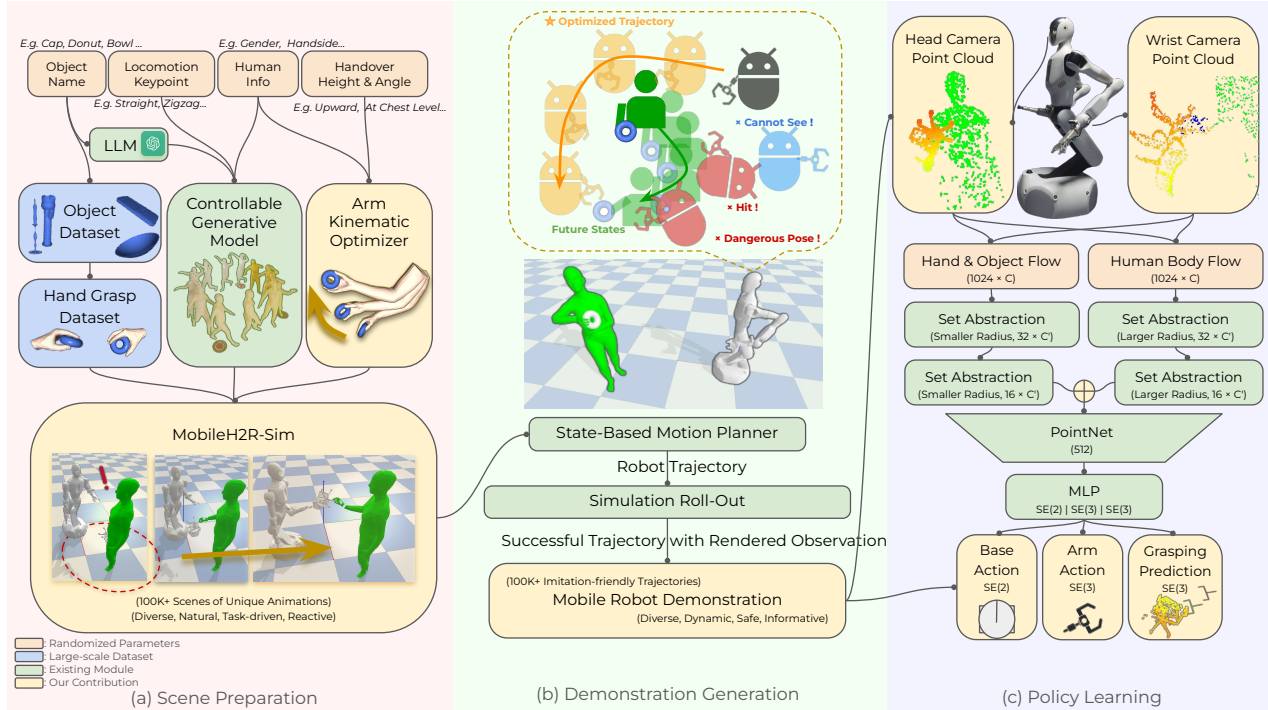


Figure 2. **The overview of our framework.** First, we propose an automatic pipeline to scale up synthetic and diverse full-body motion data for the handover task by integrating various synthetic digital asset libraries, generative models, and useful toolkits. Second, we introduce an automatic pipeline to scale up mobile robot demonstrations for safety and imitation-friendliness. Our approach aims to avoid collisions while enhancing the vision-action correlation through carefully designed loss functions. Third, we employ a 4D imitation learning policy to learn 9D coordinated arm-base actions. We process point clouds of both objects and human bodies by modified PointNet++.

without engaging in the handover. The phase transition is triggered when the robot approaches within a specific range or when the pre-handover time limit is reached. Once the handover movement is completed, all motion ceases, marking the end of the mobile handover task.

Several technical enhancements are incorporated into our approach. We utilize large digital asset libraries such as ShapeNet [1], which provides 8,836 synthetic objects, and Acronym [12], which offers corresponding grasping pose sets. To capture the nuanced hand poses necessary for a secure grip, we leverage DexGraspNet [47]. Furthermore, to ensure that the full-body movements generated by the generative model are object-aware, we resort to the large language model [37] to generate motion prompts that align with the semantic attributes of the object.

### 3.2. Safe and Imitation-friendly Demonstration

GenH2R [49] has shown that distillation-friendly demonstrations are crucial for vision-based closed-loop policy learning in fixed-base handover. Due to the robot’s increased freedom and the resulting safety concerns, adapting this to mobile-base handover is challenging and requires finer-tuned strategies. Therefore, we aim to address two key questions in scalable demonstration generation for mobile-base handover: how to ensure safe human robot interac-

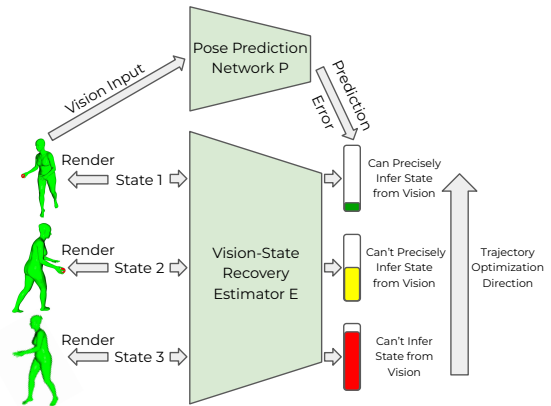


Figure 3. **Visualization for the vision neural loss.** The Pose Prediction Network takes vision inputs and predicts the object pose. The prediction error is defined as the vision neural loss. The Vision-State Recovery Estimator takes states as input and estimates the vision neural loss, guiding the state-based trajectory optimization towards imitation-friendly demonstration generation.

tion and how to generate imitation-friendly demonstrations in mobile environments.

Specifically, CHOMP [40], an optimization-based planner is used as our expert planner, which is commonly applied directly or indirectly in recent handover research [4,

5, 49] to optimize robot trajectories. This planner offers simplicity and flexibility, allowing us to refine the initial trajectory through gradient descent to meet various objectives. To support this planner, we provide privileged scene knowledge, including the object’s 6D pose, hand and human poses, and candidate target object grasps generated via physics simulation [12] at any moment.

For safety, we employ future obstacle avoidance to prevent collisions between the human and the robot over a time window, rather than just at the current timestamp. Traditional obstacle losses focus on immediate collisions, typically relying on the human’s signed distance field and the robot’s collision points at the current time, which may result in unavoidable collisions at future timestamps. In contrast, by utilizing oracle information, we are able to foresee the future positions of both the human and the robot, which enables us to calculate the obstacle loss at each future moment, proactively avoid potential collisions, and generate smoother and more natural robot movements.

In addition, we constrain the robot’s final position, ensuring it stops in front of the person for a visible, face-to-face handover. This approach helps avoid movements that, while technically collision-free, could feel unsafe to the human—such as when the robot stands behind the person and extends its arm around to grasp an object from the front.

To ensure imitation-friendly learning for the visuomotor policy, we must ensure that the vision-to-action mapping is learnable. Since the demonstration generator essentially models the mapping between oracle states and actions without considering vision, our key insight is that if vision can effectively recover the state, the association between vision and action can be enhanced, making imitation learning easier. For example, if an object is occluded due to camera limitations, the demonstration may still succeed, but the policy cannot effectively learn from this visual input for imitation.

To establish a clear vision-to-state-to-action pathway, we need to identify crucial state information that links the vision-action correlation. We find that object pose is a key oracle because knowing the object’s position enables effective grasping actions. If we can recover the object’s pose from vision, we can bridge the vision-to-state-to-action learning path. Specifically, we train a pose prediction network  $P$  that takes vision input and predicts the object pose, defining the vision neural loss as the difference between the predicted pose and the ground truth pose. If the vision input accurately recovers the object pose, the loss is low. Unfortunately, visual inputs rendered from simulations (such as PyBullet [7] or IsaacGym [31]) are often non-differentiable, meaning that the neural loss cannot propagate gradients for trajectory optimization. To address this, we trained a vision-state recovery estimator  $E$ , which estimates the vision neural loss defined by  $P$  for each state. For state-vision pairs,  $E$  takes states as input, and predicts the vision neural loss

for the vision inputs given by  $P$ . Now vision neural loss estimated from  $E$  can propagate gradients to the states, allowing for trajectory optimization, as shown in Figure 3.

We can also add some heuristic designs to ensure visibility with the aim of enhancing the vision-action correlation, such as keeping the camera constantly oriented towards the object. However, based on experimental results, overly hacky designs often fail to capture the subtlety of the vision-action relationship, disrupt the robot’s normal posture and trajectory, and lack generalizability. In contrast, our neural vision loss, by modeling the state, implicitly optimizes a better vision-action correlation.

### 3.3. Imitation for Coordinated Base-Arm Actions

Recent human-to-robot handover approaches focus mainly on the interaction between the human hand and the robot’s end-effector, often neglecting contextual factors such as the human’s motion and posture. Many methods crop only the hand and object point clouds [5, 53], which could introduce safety risks. Additionally, state-of-the-art models [49] typically focus on 6D egocentric actions at the arm’s end-effector, ignoring the robot’s base coordination—critical for mobile robots. To address these challenges, we propose a scene-fused 4D imitation learning approach that integrates full-body coordination and vision-action dynamics for more holistic human robot interactions.

To fully leverage the scene information, we combine the point clouds from the front and wrist cameras, which are segmented into objects, hands, and human body components, and align them with the robot’s end-effector frame. Our policy uses these point clouds as inputs and outputs an egocentric 6D action for the robotic arm and an egocentric 3D action for the mobile base. Inspired by GenH2R [49], we balance the policy’s 4D learning capabilities with real-world inference speed by reconstructing the point cloud at each timestamp and calculating flow information between consecutive point clouds using the Iterative Closest Point registration algorithm. This method approximates the previous timestamp’s point cloud coordinates, enhancing the current point cloud features with 4D information. To extract global features from point clouds enriched with 4D information, we typically use a PointNet++ [39] encoder. However, due to the differing spatial scales between the human body and hand-object point clouds, using a single set abstraction layer for the entire point cloud often causes the FPS algorithm to prioritize points from the human body. To address this, we apply set abstraction layers with distinct sampling radii for the human body and hand-object regions. In the final PointNet layer, we concatenate these features to obtain a unified global feature representation.

To ensure coordinated movement between the base and the robotic arm, we directly input the unified global feature into an MLP layer, which decodes base and arm movements

	m0			n0			s0		
	Success	Time	AS	Success	Time	AS	Success	Time	AS
Grasp Selection + Trajectory Planning	40.20	11.75	8.70	34.80	12.83	5.02	40.97	9.61	14.71
GenH2R	4.80	6.93	2.58	3.10	8.66	1.31	40.97	4.93	27.5
GenH2R (reprod.)	46.80	<b>6.58</b>	26.27	32.90	7.03	17.48	61.11	<b>4.67</b>	42.09
Ours	<b>63.80</b>	6.82	<b>34.81</b>	<b>53.40</b>	<b>6.94</b>	<b>28.68</b>	<b>77.78</b>	5.23	<b>50.65</b>

Table 1. **Evaluation on different methods.** We compare our method against baselines across three test sets: the relatively simple human-involved scenario "m0", complex scenarios "n0", and real mocap data "s0". The "time" metric combines both computation and execution time. Since computation time varies depending on GPU and CPU configurations, we standardized it using an idle RTX 3090 with 32 CPU cores. Our policy outperforms the baselines in success rate and average success, while maintaining relatively low time cost.

simultaneously. The output is supervised using coordinated movements from the demonstrations, resulting in the losses  $\mathcal{L}_{\text{base}}$  and  $\mathcal{L}_{\text{arm}}$ . Additionally, an auxiliary task is employed to predict the object’s grasping pose, enabling the robotic arm to better anticipate the target position. Our final loss function is defined as  $\mathcal{L} = \lambda_1 \mathcal{L}_{\text{base}} + \lambda_2 \mathcal{L}_{\text{arm}} + \lambda_3 \mathcal{L}_{\text{pred}}$ , where  $\lambda_1$ ,  $\lambda_2$ , and  $\lambda_3$  are used to balance the losses. This distillation approach enables our policy to naturally execute coordinated base-arm actions, generalizing effectively to dynamic scenarios.

## 4. Experiments

**Dataset.** (1) As described in Section 3.1, Our data generation pipeline enables the creation of a large number of complex synthetic H2R handover scenes, incorporating custom human animations and 8,836 diverse objects from ShapeNet [1]. We designed two setups, "m0" and "n0", to represent different levels of diversity in human motion generation. In "m0", the human approaches straightforwardly to hand over the object, simulating a relatively simple scenario. In "n0", the human performs the handover with more complex body motions, trajectories, and speeds, such as sitting, running, descending stairs, or dancing, to mimic more varied real-world handover situations. Each setup includes 100k training scenes and 1k testing scenes. Each handover action includes a 6s pre-handover phase with natural movements, followed by a 1.05s handover phase for object transfer. The transition to the handover phase occurs when the human-robot distance falls below a 1m threshold or when the pre-handover phase has elapsed. (2) To incorporate more real-world handover scenes into MobileH2R-Sim for evaluation, we use the DexYCB [2] dataset from Handover-Sim [3], which provides 1,000 real-world H2R handover scenes and 20 objects. As this dataset captures only hand and object motion data, we add a human body model to align with our setup without altering the existing hand or object trajectories. We use the simultaneous "s0" setup, containing 720 training scenes and 144 testing scenes.

**Metrics.** We adhere to the GenH2R [49] evaluation protocol. A successful handover requires securely grasping the object from the human hand without any collision. Failure cases include human contact, object drop, and timeout

( $T_{\text{max}} = 15s$ ). We report the success rate and the time. It is noted that the "time" metric consists of inference time (policy action computation) and execution time (action execution in simulation). While GenH2R only considers inference time, we include both, offering a more accurate reflection of real-world performance. To evaluate both success rate and completion efficiency, we use AS (Average Success), akin to AP (Average Precision):

$$\text{AS} = \int_0^1 \text{Success}(t) dt \quad (1)$$

where  $\text{Success}(t)$  is success rate considering only successful cases within  $t \cdot T_{\text{max}}$ . This method can better evaluate success-time relations which is suitable in HRI scenarios.

### 4.1. Evaluation on Different Methods

**Setup.** To ensure a fair comparison between baseline methods and our imitation policies powered by imitation-friendly demonstrations, we train all methods on the 10k "n0" training scenes and evaluate them on three testing sets: "m0", "n0", and "s0".

**Baselines.** "Grasp Selection + Trajectory Planning" is a non-end-to-end, straightforward method. The point cloud input is used to predict the target grasping pose, either via GraspNet [14, 15] or by matching current visual input with the object’s ground truth grasping pose [12]. Based on it, motion planning is performed at each time step. Although time-consuming, this baseline is widely adopted for its ease of implementation. GenH2R is an end-to-end approach for fixed-base handover tasks, converting the current hand-object point cloud into robotic arm motions. However, it lacks a full-body robot and only outputs 6D arm actions. We can extend it to base-arm actions by solving full-body inverse kinematics. Additionally, GenH2R’s environment does not include humanoid interaction. We either use the pre-trained GenH2R model or retrain it in "n0" (GenH2R(reprod.)) to learn 6D arm actions with the mobile base and incorporate collision-free demonstrations.

**An end-to-end framework models the HRI scenario more effectively.** Compared to "Grasp Selection + Trajectory Planning", our method achieves a 26.3% higher success rate, reduces time by 5.06s, and increases average suc-

Num. of Demos / training set	m0	n0	s0
100k, n0	65.6↑	56.6↑	82.6↑
	53.4↓	42.3↓	57.6↓
10k, n0	63.8	53.4	77.8
10k, m0	62.0↓	45.3↓	76.4↓
10k, s0	35.3↓	22.0↓	34.0↓

Table 2. **Evaluation on varying demonstration numbers and Assets.** We compare the policy’s success rate across three testing sets, examining the impact of different demonstration sizes within **brown braces** and asset variations within **green braces**.

cess by 28.6% on average. The non-end-to-end method fails mainly due to collisions with human, as it plans based only on the current step and doesn’t anticipate human movements to avoid them in advance. Frequent planning steps also increase computation time, with our policy requiring about 0.003s for inference, while motion planning usually takes over 0.1s. These results show that an end-to-end framework better captures the global context, though more complex methods like MPC could consider more factors, they often lack scalability.

**Human involvement and mobility are crucial.** For the baseline GenH2R, handover success is challenging, with frequent human collisions in the “m0” and “n0” test sets due to the lack of awareness of complex human motion and intent. In contrast, GenH2R(reprod.) benefits from demonstrations that implicitly avoid collisions, improving success rates by 42.0%, 29.8%, and 20.1% across the three test sets. However, it only learns 6D arm actions and computes 3D base actions via inverse kinematics. Our approach, which incorporates human information and considers base-arm coordination, achieves further success rate improvements of 17.0%, 20.5%, and 16.7%. This shows that learning base-arm coordination is essential. A strategy suitable for a fixed-base arm cannot be directly applied to a mobile robot without accounting for its specific configuration. We also show visualizations in Figure 4 (a).

## 4.2. Evaluation on Data Scaling

As shown in Table 2, we evaluate the impact of scaling from two perspectives: demonstration scaling and asset scaling.

When comparing different demonstration sizes trained on the same dataset “n0”, We observe that using 100k demonstrations increases the success rate by 3.3% on average compared to using 10k demonstrations, while using 1k demonstrations leads to a 13.9% decrease in success rate. These results highlight the importance of dataset size in our imitation learning paradigm. Our large-scale synthetic data and efficient demonstration pipeline mitigate concerns about limited datasets affecting generalization.

On the other hand, using the unscalable mocap dataset “s0” results in a significant drop in the success rate by 34.6% on average. When trained on the simpler human-

Demo strategies	m0	n0	s0
w/o future obstacle avoidance	58.7	48.5	75.7
w/o final pose constraints	58.4	43.2	69.4
w/o imitation-friendly loss	56.8	46.4	56.9
with camera orient-based loss	54.0	42.8	56.0
safety concern + vision neural loss	<b>63.8</b>	<b>53.4</b>	<b>77.8</b>

Table 3. **Evaluation on different demonstration generation strategies.** We compare the policy’s success rate across three testing sets. They all trained on “n0”.

involved “m0” dataset, the policy performs well on the simple testing set, with a small drop in success rates of 1.8% and 1.4% for “m0” and “s0”. However, in more complex scenarios, the success rate decreases by 8.1%. This shows that the complexity and diversity of human assets are crucial for the policy’s ability to handle more challenging tasks.

The above results validate our assumption that, for HRI tasks, **increasing the number of demonstrations and the diversity of assets is key to improving policy performance.** This also highlights the value of our scalable framework.

## 4.3. Evaluation on Demonstration Strategies

As shown in Table 3, we evaluate different demonstration strategies in terms of safety and imitation-friendliness.

Without future obstacle avoidance, the policy’s success rate decreases by an average of 4.0%, and the human contact rate increases from 10.9% to 16.1%. Without final pose constraints, the success rate decreases by an average of 8.0%, and the contact rate rises to 19.8%. These results highlight that demonstrations with a simple safety design can significantly reduce human collisions, which are the most critical failures to avoid, as compared to failures such as object drops or timeouts.

For the imitation-friendly purpose, we find that without encouraging easy vision-to-action learning, the success rate drops by 11.6%. The loss for training the policy is much higher when dealing with irrational vision-action pairs. When we manually design an orientation loss for the robot camera to keep it continuously focused on the object, the policy performs worse than one without the orientation constraint. We check the generated demonstrations and notice that many of them attempt to align the object’s angle, leading to stagnation and discontinuity in actions, which results in even more irrational vision-action pairs. Therefore, generating distillation-friendly demonstrations requires a balance between various considerations.

## 4.4. Ablations

As depicted in Table 4, we make ablations on different designs for our imitation policy. The absence of flow information leads to a 12.1% decrease in success rate, emphasizing the importance of utilizing 4D data. Without human infor-

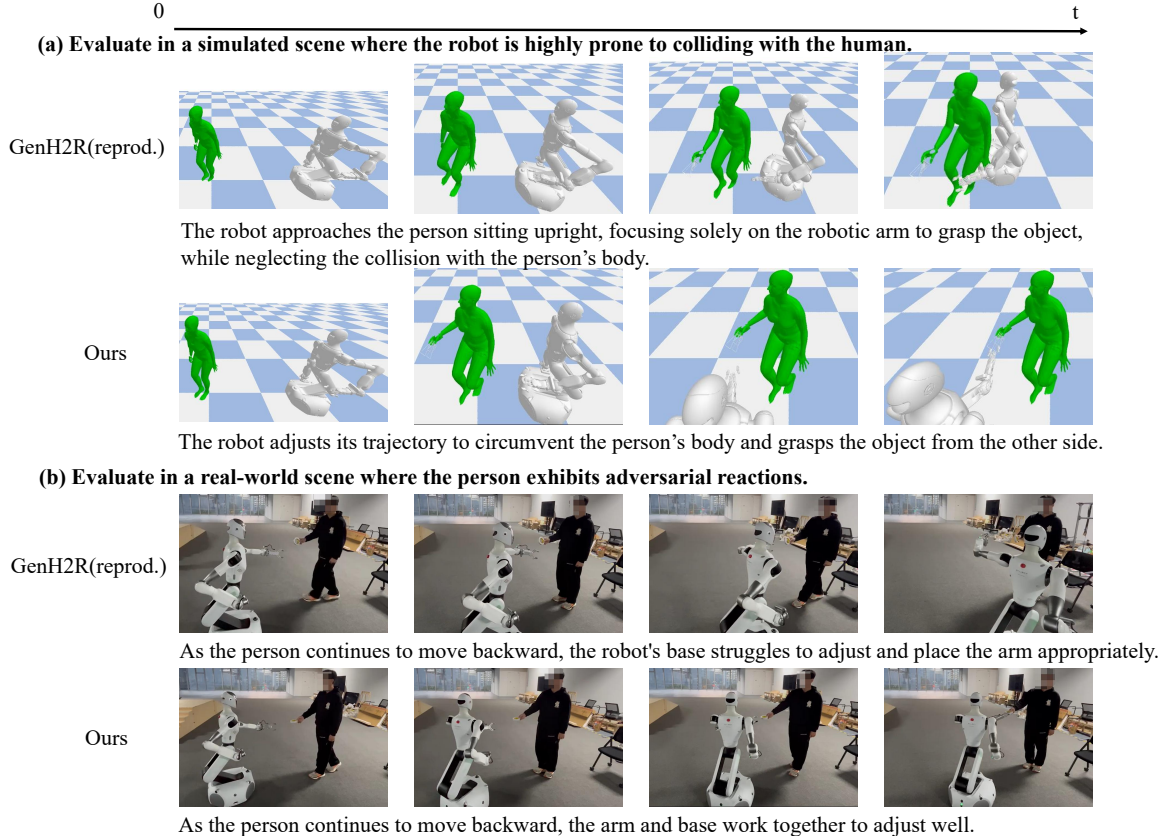


Figure 4. **Qualitative results.** We compare different methods in detail in the simulated scene and the real-world scene.

Methods	m0	n0	s0
w/o flow	58.0	47.2	53.5
w/o human	51.3	48.7	57.6
w/o coordinated action	51.0	41.7	48.9
Ours	<b>63.8</b>	<b>53.4</b>	<b>77.8</b>

Table 4. **Ablations on different policy designs.** We conduct ablations on various modules, including flow information, human information, and coordinated base-arm actions.

Methods	m0	n0
GenH2R(reprod.) [49]	12 / 30 (40.0%)	9 / 30 (30.0%)
Ours	24 / 30 ( <b>80.0%</b> )	19 / 30 ( <b>63.3%</b> )

Table 5. **Sim-to-real experiments.** We report the success rate of our method and GenH2R(reprod.) in two different settings.

mation, the success rate drops by 12.5%, highlighting the need to consider human-related context in HRI tasks. When decoding the arm and base actions separately using two independent networks (e.g., two PointNet++), we observe a dramatic 17.8% decrease in success rate, demonstrating the necessity of decoding both actions simultaneously.

#### 4.5. Real World Experiments

**Sim-to-Real Transfer.** we deploy the models trained in the simulation on a real mobile robot, Galbot G1, equipped with an omnidirectional wheel chassis, a 7-DOF robotic

arm, a head depth camera, and a wrist-mounted depth camera. We use SAM2 [41] to segment the point cloud data from the cameras, which is then fed into the policy to generate 9D egocentric actions for both the base and the left arm. The robot's movements are controlled using a position controller. A user study compares our method against the GenH2R(reprod.) approach. Further details are provided in the supplementary material.

**User Study.** We compare our method with GenH2R(reprod.) across 6 objects in 2 different settings. In the simple setting, users directly hand over the object to mimic "m0". In the complex setting, users may sit, go downstairs, or perform adversarial actions to mimic "n0". The results are reported in Table 5 and visualizations are shown in Figure 4(b). We observe that our model outperforms in completing the handover process across different objects and scenarios.

## 5. Conclusion

In this work, we present the MobileH2R framework for scaling the learning of generalizable human-to-mobile-robot (H2MR) handover. We introduce a new simulation environment for this task and a scalable pipeline for generating diverse synthetic full-body human motion data. Additionally, we propose an automatic method for creating safe,



imitation-friendly demonstrations, enabling a 4D imitation learning approach to train coordinated base-arm actions. Our experiments show that generalizable handover skills can be developed in simulators using high-quality synthetic data, without the need for real-world data. We validate the approach both in the simulator and in the real world.

## References

- [1] Angel X Chang, Thomas Funkhouser, Leonidas Guibas, Pat Hanrahan, Qixing Huang, Zimo Li, Silvio Savarese, Manolis Savva, Shuran Song, Hao Su, et al. Shapenet: An information-rich 3d model repository. *arXiv preprint arXiv:1512.03012*, 2015. 4, 6
- [2] Yu-Wei Chao, Wei Yang, Yu Xiang, Pavlo Molchanov, Ankur Handa, Jonathan Tremblay, Yashraj S Narang, Karl Van Wyk, Umar Iqbal, Stan Birchfield, et al. Dexycb: A benchmark for capturing hand grasping of objects. In *Proceedings of the IEEE/CVF Conference on Computer Vision and Pattern Recognition*, pages 9044–9053, 2021. 1, 2, 6
- [3] Yu-Wei Chao, Chris Paxton, Yu Xiang, Wei Yang, Balakumar Sundaralingam, Tao Chen, Adithyavairavan Murali, Maya Cakmak, and Dieter Fox. Handoversim: A simulation framework and benchmark for human-to-robot object handovers. In *2022 International Conference on Robotics and Automation (ICRA)*, pages 6941–6947. IEEE, 2022. 1, 2, 6
- [4] Sammy Christen, Lan Feng, Wei Yang, Yu-Wei Chao, Otmar Hilliges, and Jie Song. Synh2r: Synthesizing hand-object motions for learning human-to-robot handovers. *arXiv preprint arXiv:2311.05599*, 2023. 2, 4
- [5] Sammy Christen, Wei Yang, Claudia Pérez-D’Arpino, Otmar Hilliges, Dieter Fox, and Yu-Wei Chao. Learning human-to-robot handovers from point clouds. In *Proceedings of the IEEE/CVF Conference on Computer Vision and Pattern Recognition*, pages 9654–9664, 2023. 2, 5
- [6] Gianluca Corsini, Martin Jacquet, Hemjyoti Das, Amr Afifi, Daniel Sidobre, and Antonio Franchi. Nonlinear model predictive control for human-robot handover with application to the aerial case. In *2022 IEEE/RSJ International Conference on Intelligent Robots and Systems (IROS)*, pages 7597–7604. IEEE, 2022. 2
- [7] Erwin Coumans and Yunfei Bai. Pybullet, a python module for physics simulation for games, robotics and machine learning. <http://pybullet.org>, 2016–2021. 5
- [8] Murtaza Dalal, Ajay Mandlekar, Caelan Garrett, Ankur Handa, Ruslan Salakhutdinov, and Dieter Fox. Imitating task and motion planning with visuomotor transformers. *arXiv preprint arXiv:2305.16309*, 2023. 3
- [9] Matt Deitke, Dustin Schwenk, Jordi Salvador, Luca Weihs, Oscar Michel, Eli VanderBilt, Ludwig Schmidt, Kiana Ehsani, Aniruddha Kembhavi, and Ali Farhadi. Objaverse: A universe of annotated 3d objects. In *Proceedings of the IEEE/CVF Conference on Computer Vision and Pattern Recognition*, pages 13142–13153, 2023. 2
- [10] Matt Deitke, Ruoshi Liu, Matthew Wallingford, Huong Ngo, Oscar Michel, Aditya Kusupati, Alan Fan, Christian Laforte, Vikram Voleti, Samir Yitzhak Gadre, et al. Objaverse-xl: A universe of 10m+ 3d objects. *Advances in Neural Information Processing Systems*, 36, 2024. 2
- [11] Haonan Duan, Yifan Yang, Daheng Li, and Peng Wang. Human–robot object handover: Recent progress and future direction. *Biomimetic Intelligence and Robotics*, 4(1):100145, 2024. 2
- [12] Clemens Eppner, Arsalan Mousavian, and Dieter Fox. Acronym: A large-scale grasp dataset based on simulation. In *2021 IEEE International Conference on Robotics and Automation (ICRA)*, pages 6222–6227. IEEE, 2021. 4, 5, 6, 14
- [13] Zicong Fan, Omid Taheri, Dimitrios Tzionas, Muhammed Kocabas, Manuel Kaufmann, Michael J Black, and Otmar Hilliges. Arctic: A dataset for dexterous bimanual hand-object manipulation. In *Proceedings of the IEEE/CVF Conference on Computer Vision and Pattern Recognition*, pages 12943–12954, 2023. 2
- [14] Hao-Shu Fang, Chenxi Wang, Minghao Gou, and Cewu Lu. Graspnet-1billion: A large-scale benchmark for general object grasping. In *Proceedings of the IEEE/CVF Conference on Computer Vision and Pattern Recognition (CVPR)*, pages 11444–11453, 2020. 6
- [15] Hao-Shu Fang, Minghao Gou, Chenxi Wang, and Cewu Lu. Robust grasping across diverse sensor qualities: The graspnet-1billion dataset. *The International Journal of Robotics Research*, 2023. 6
- [16] Hao-Shu Fang, Chenxi Wang, Hongjie Fang, Minghao Gou, Jirong Liu, Hengxu Yan, Wenhai Liu, Yichen Xie, and Cewu Lu. Anygrasp: Robust and efficient grasp perception in spatial and temporal domains. *IEEE Transactions on Robotics*, 2023. 2
- [17] Caelan Reed Garrett, Rohan Chitnis, Rachel Holladay, Beomjoon Kim, Tom Silver, Leslie Pack Kaelbling, and Tomás Lozano-Pérez. Integrated task and motion planning. *Annual review of control, robotics, and autonomous systems*, 4:265–293, 2021. 3
- [18] Kristen Grauman, Andrew Westbury, Eugene Byrne, Zachary Chavis, Antonino Furnari, Rohit Girdhar, Jackson Hamburger, Hao Jiang, Miao Liu, Xingyu Liu, et al. Ego4d: Around the world in 3,000 hours of egocentric video. In *Proceedings of the IEEE/CVF Conference on Computer Vision and Pattern Recognition*, pages 18995–19012, 2022. 3
- [19] Huy Ha, Pete Florence, and Shuran Song. Scaling up and distilling down: Language-guided robot skill acquisition. *arXiv preprint arXiv:2307.14535*, 2023. 3
- [20] Yu-Yun Huang and Kai-Tai Song. Human-to-robot handover control of an autonomous mobile robot based on hand-masked object pose estimation. *IEEE Robotics and Automation Letters*, 9(9):7851–7858, 2024. 2
- [21] Catalin Ionescu, Dragos Papava, Vlad Olaru, and Cristian Sminchisescu. Human3.6m: Large scale datasets and predictive methods for 3d human sensing in natural environments. *IEEE Transactions on Pattern Analysis and Machine Intelligence*, 36(7):1325–1339, 2014. 3
- [22] Snehal Jauhri, Jan Peters, and Georgia Chalvatzaki. Robot learning of mobile manipulation with reachability behavior priors. *IEEE Robotics and Automation Letters*, 7(3):8399–8406, 2022. 3

- [23] Korrawe Karunratanakul, Konpat Preechakul, Supasorn Suwajanakorn, and Siyu Tang. Guided motion diffusion for controllable human motion synthesis, 2023. 2, 3, 12, 13
- [24] Chengshu Li, Fei Xia, Roberto Martin-Martín, and Silvio Savarese. Hrl4in: Hierarchical reinforcement learning for interactive navigation with mobile manipulators. In *Conference on Robot Learning*, pages 603–616. PMLR, 2020. 3
- [25] Yi Li, Gu Wang, Xiangyang Ji, Yu Xiang, and Dieter Fox. Deepim: Deep iterative matching for 6d pose estimation. In *Proceedings of the European Conference on Computer Vision (ECCV)*, pages 683–698, 2018. 14
- [26] Jing Lin, Ailing Zeng, Shunlin Lu, Yuanhao Cai, Ruimao Zhang, Haoqian Wang, and Lei Zhang. Motion-x: A large-scale 3d expressive whole-body human motion dataset, 2024. 2, 3
- [27] Minghuan Liu, Zixuan Chen, Xuxin Cheng, Yandong Ji, Rihao Qiu, Ruihan Yang, and Xiaolong Wang. Visual whole-body control for legged loco-manipulation. *arXiv preprint arXiv:2403.16967*, 2024. 3
- [28] Yunze Liu, Yun Liu, Che Jiang, Kangbo Lyu, Weikang Wan, Hao Shen, Boqiang Liang, Zhoujie Fu, He Wang, and Li Yi. Hoi4d: A 4d egocentric dataset for category-level human-object interaction. In *Proceedings of the IEEE/CVF Conference on Computer Vision and Pattern Recognition*, pages 21013–21022, 2022. 2
- [29] Matthew Loper, Naureen Mahmood, Javier Romero, Gerard Pons-Moll, and Michael J. Black. SMPL: A skinned multi-person linear model. *ACM Trans. Graphics (Proc. SIGGRAPH Asia)*, 34(6):248:1–248:16, 2015. 13
- [30] Naureen Mahmood, Nima Ghorbani, Nikolaus F. Troje, Gerard Pons-Moll, and Michael J. Black. AMASS: Archive of motion capture as surface shapes. In *International Conference on Computer Vision*, pages 5442–5451, 2019. 2, 3
- [31] Viktor Makoviychuk, Lukasz Wawrzyniak, Yunrong Guo, Michelle Lu, Kier Storey, Miles Macklin, David Hoeller, Nikita Rudin, Arthur Allshire, Ankur Handa, and Gavriel State. Isaac gym: High performance gpu-based physics simulation for robot learning, 2021. 5
- [32] Michael James McDonald and Dylan Hadfield-Menell. Guided imitation of task and motion planning. In *Conference on Robot Learning*, pages 630–640. PMLR, 2022. 3
- [33] Emi Moriuchi and Samantha Murdy. The role of robots in the service industry: Factors affecting human-robot interactions. *International Journal of Hospitality Management*, 118:103682, 2024. 2
- [34] James F Mullen Jr and Dinesh Manocha. Towards robots that know when they need help: Affordance-based uncertainty for large language model planners. *arXiv preprint arXiv:2403.13198*, 2024. 3
- [35] Alexander Obaigbena, Oluwaseun Augustine Lottu, Ejike David Ugwuanyi, Boma Sonimitem Jacks, Enoch Oluwademilade Sodiya, and Obinna Donald Daraojimba. Ai and human-robot interaction: A review of recent advances and challenges. *GSC Advanced Research and Reviews*, 18(2):321–330, 2024. 2
- [36] Abby O’Neill, Abdul Rehman, Abhinav Gupta, Abhiram Maddukuri, Abhishek Gupta, Abhishek Padalkar, Abraham Lee, Acorn Pooley, Agrim Gupta, Ajay Mandlekar, et al. Open x-embodiment: Robotic learning datasets and rt-x models. *arXiv preprint arXiv:2310.08864*, 2023. 3
- [37] OpenAI. Gpt-4, 2023. Accessed: 2024-11-15. 4, 13
- [38] Georgios Pavlakos, Vasileios Choutas, Nima Ghorbani, Timo Bolkart, Ahmed A. A. Osman, Dimitrios Tzionas, and Michael J. Black. Expressive body capture: 3D hands, face, and body from a single image. In *Proceedings IEEE Conf. on Computer Vision and Pattern Recognition (CVPR)*, pages 10975–10985, 2019. 13
- [39] Charles Ruizhongtai Qi, Li Yi, Hao Su, and Leonidas J Guibas. Pointnet++: Deep hierarchical feature learning on point sets in a metric space. *Advances in neural information processing systems*, 30, 2017. 5
- [40] Nathan Ratliff, Matt Zucker, J Andrew Bagnell, and Siddhartha Srinivasa. Chomp: Gradient optimization techniques for efficient motion planning. In *2009 IEEE international conference on robotics and automation*, pages 489–494. IEEE, 2009. 4
- [41] Nikhila Ravi, Valentin Gabeur, Yuan-Ting Hu, Ronghang Hu, Chaitanya Ryali, Tengyu Ma, Haitham Khedr, Roman Rädle, Chloe Rolland, Laura Gustafson, Eric Mintun, Junting Pan, Kalyan Vasudev Alwala, Nicolas Carion, Chaoyuan Wu, Ross Girshick, Piotr Dollár, and Christoph Feichtenhofer. Sam 2: Segment anything in images and videos. *arXiv preprint arXiv:2408.00714*, 2024. 8, 17
- [42] Javier Romero, Dimitrios Tzionas, and Michael J. Black. Embodied hands: Modeling and capturing hands and bodies together. *ACM Transactions on Graphics, (Proc. SIGGRAPH Asia)*, 36(6), 2017. 13
- [43] Szymon Rusinkiewicz and Marc Levoy. Efficient variants of the icp algorithm. In *Proceedings third international conference on 3-D digital imaging and modeling*, pages 145–152. IEEE, 2001. 15
- [44] Shuran Song, Andy Zeng, Johnny Lee, and Thomas Funkhouser. Grasping in the wild: Learning 6dof closed-loop grasping from low-cost demonstrations. *IEEE Robotics and Automation Letters*, 5(3):4978–4985, 2020. 3
- [45] Jilong Wang, Javokhirbek Rajabov, Chaoyi Xu, Yiming Zheng, and He Wang. Quadwb: Generalizable quadrupedal whole-body grasping, 2024. 3
- [46] Lirui Wang, Yiyang Ling, Zhecheng Yuan, Mohit Shridhar, Chen Bao, Yuzhe Qin, Bailin Wang, Huazhe Xu, and Xiaolong Wang. Gensim: Generating robotic simulation tasks via large language models. *arXiv preprint arXiv:2310.01361*, 2023. 3
- [47] Ruicheng Wang, Jialiang Zhang, Jiayi Chen, Yinzheng Xu, Puhao Li, Tengyu Liu, and He Wang. Dexgraspnet: A large-scale robotic dexterous grasp dataset for general objects based on simulation, 2023. 4, 13
- [48] Yufei Wang, Zhou Xian, Feng Chen, Tsun-Hsuan Wang, Yian Wang, Katerina Fragkiadaki, Zackory Erickson, David Held, and Chuang Gan. Robogen: Towards unleashing infinite data for automated robot learning via generative simulation. *arXiv preprint arXiv:2311.01455*, 2023. 3
- [49] Zifan Wang, Junyu Chen, Ziqing Chen, Pengwei Xie, Rui Chen, and Li Yi. Genh2r: Learning generalizable human-to-robot handover via scalable simulation demonstration and

- imitation. In *Proceedings of the IEEE/CVF Conference on Computer Vision and Pattern Recognition (CVPR)*, pages 16362–16372, 2024. [2](#), [3](#), [4](#), [5](#), [6](#), [8](#), [14](#), [18](#)
- [50] Fei Xia, Chengshu Li, Roberto Martín-Martín, Or Litany, Alexander Toshev, and Silvio Savarese. Relmogen: Leveraging motion generation in reinforcement learning for mobile manipulation. *arXiv preprint arXiv:2008.07792*, 2020. [3](#)
- [51] Jiannan Xiang, Tianhua Tao, Yi Gu, Tianmin Shu, Zirui Wang, Zichao Yang, and Zhiting Hu. Language models meet world models: Embodied experiences enhance language models. *Advances in neural information processing systems*, 36, 2024. [3](#)
- [52] Ruihan Yang, Yejin Kim, Rose Hendrix, Aniruddha Kembhavi, Xiaolong Wang, and Kiana Ehsani. Harmonic mobile manipulation. *arXiv preprint arXiv:2312.06639*, 2023. [3](#)
- [53] Wei Yang, Chris Paxton, Arsalan Mousavian, Yu-Wei Chao, Maya Cakmak, and Dieter Fox. Reactive human-to-robot handovers of arbitrary objects. In *2021 IEEE International Conference on Robotics and Automation (ICRA)*, pages 3118–3124. IEEE, 2021. [2](#), [5](#)
- [54] Ruolin Ye, Wenqiang Xu, Zhendong Xue, Tutian Tang, Yanfeng Wang, and Cewu Lu. H2o: A benchmark for visual human-human object handover analysis. In *Proceedings of the IEEE/CVF International Conference on Computer Vision*, pages 15762–15771, 2021. [2](#)
- [55] Naoki Yokoyama, Alex Clegg, Joanne Truong, Eric Underlander, Tsung-Yen Yang, Sergio Arnaud, Sehoon Ha, Dhruv Batra, and Akshara Rai. Asc: Adaptive skill coordination for robotic mobile manipulation. *IEEE Robotics and Automation Letters*, 9(1):779–786, 2023. [3](#)
- [56] Gu Zhang, Hao-Shu Fang, Hongjie Fang, and Cewu Lu. Flexible handover with real-time robust dynamic grasp trajectory generation. *arXiv preprint arXiv:2308.15622*, 2023. [2](#)

# MobileH2R: Learning Generalizable Human to Mobile Robot Handover Exclusively from Scalable and Diverse Synthetic Data (Supplementary Material)

The supplementary material provides additional details about various aspects of our method and experiments. Refer to the table of contents below for an overview. Section A offers further details on our framework and methodologies. Sections B and C elaborate on the experimental setups and results in simulation and real-world scenarios, respectively. Section D discusses the limitations of our work and explores potential future research directions for human-to-mobile-robot handovers and broader human-robot interactions.

Additionally, we have attached a video that provides an overview of our method, along with extensive demonstrations in both simulation and real-world scenarios.

We are committed to contributing to the research community and will release our code publicly in the near future.

## Contents

<b>1. Introduction</b>	<b>1</b>
<b>2. Related Work</b>	<b>2</b>
2.1. Human-to-Robot Handovers . . . . .	2
2.2. Mobile Robot Manipulation . . . . .	3
2.3. Scaling up Demonstrations for Imitation . . .	3
<b>3. Method</b>	<b>3</b>
3.1. MobileH2R-Sim . . . . .	3
3.2. Safe and Imitation-friendly Demonstration .	4
3.3. Imitation for Coordinated Base-Arm Actions	5
<b>4. Experiments</b>	<b>6</b>
4.1. Evaluation on Different Methods . . . . .	6
4.2. Evaluation on Data Scaling . . . . .	7
4.3. Evaluation on Demonstration Strategies . . .	7
4.4. Ablations . . . . .	7
4.5. Real World Experiments . . . . .	8
<b>5. Conclusion</b>	<b>8</b>
<b>Appendix</b>	<b>12</b>
<b>A More Method Details</b>	<b>12</b>
A.1. MobileH2R-Sim . . . . .	12
A.2. Demonstration Workflow . . . . .	14
A.3. Imitation for coordinated Based-Arm Actions	14
<b>B Simulation Experiments Details</b>	<b>15</b>
B.1. Training Details . . . . .	15
B.2. Experimental Data Details . . . . .	15
B.3. Discussion on Different Action Types . . . .	16
B.4. More ablations . . . . .	16

User

Describe actions a person might perform while walking with a particular object held in hand, each described in 8 to 15 words.

Requirements:

1. Prioritize descriptions of broad, noticeable motions over minor expressions.
2. Employ clear, descriptive verbs instead of adjectives for a vivid portrayal of actions.
3. Ensure human actions are self-contained, without any engagement with the surrounding environment.
4. Human motion had better have a logical connection with the object in their hand if possible.
5. Instead of mentioning the object, just describe where the person will put the hand with the object. Try to avoid explicitly talking about the object with "as if", "invisible" terms.
6. If the object seems too large to hold in hand...
7. Answers are supposed to follow the format...

Example:

...

Agent

...

Figure 5. **Template prompt to LLMs** to generate direct object-aware motion description for controllable motion generator.

<b>C Real World Experiments Details</b>	<b>17</b>
C.1. Setup . . . . .	17
C.2. User Study . . . . .	17

## D Limitations and Future Work 18

### A. More Method Details

#### A.1. MobileH2R-Sim

The first innovation we would like to introduce in MobileH2R-Sim is its object-aware motion prompt generation. As our human-motion generator, GMD [23], claims the capability to generate semantically correct human motion trajectories, it is theoretically possible to compose diverse motion patterns according to different objects involved in the handover task. For instance, if it is a phone, we may imagine that one will hold the phone up to one’s ear with one’s hand before handing it over. Or if it is a bottle, a more natural action would be moving it to one’s lip and taking a sip.

However, restrained by the problem setting of general

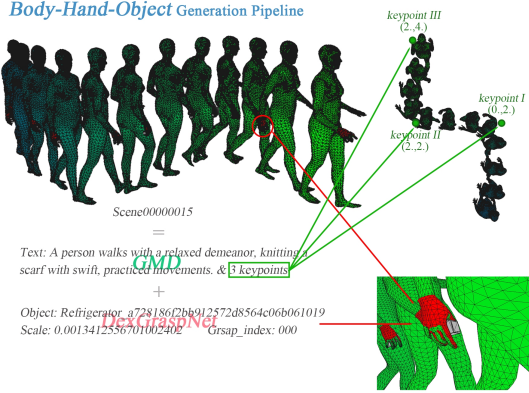


Figure 6. **Combine the body motion and the hand-object pose.** In our pipeline, the body motions are SMPL [29] parameters obtained from GMD [23], and the hand-object poses are MANO [42] parameters obtained from DexGraspNet [47]. Here we combine these parameters with SMPL-X [38] model, as well as update the object poses relative to the human body.

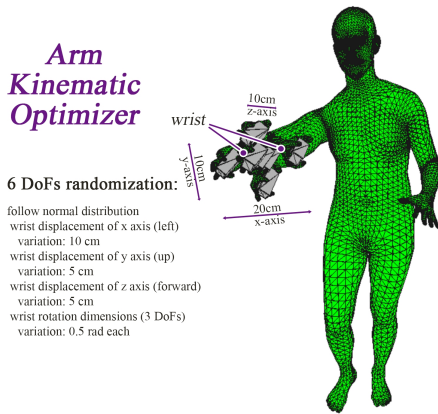


Figure 7. **Visualization for the arm kinematic optimizer.** Given the final pose of the hand, the optimizer determines the optimal hand joint parameters by optimizing under joint constraints and handover task priors. Practically, we add proper randomization to generate diverse data.

motion synthesis and mainstream data annotation, motion diffusion models at the current stage including GMD, only accept direct description as guidance, lacking the capability to understand complex semantic implications. Besides, the information of the object cannot be directly obtained by the generative model as well. So we propose to involve a large language model, like GPT4 [37], in the loop. With proper prompt 5 design, we utilize the LLM to perform (1) conceptualizing actions of a person regarding a specified item and (2) describing specific postures of a person while performing the actions. With the output as the prompt to GMD, there are two significant benefits. Firstly, the gener-

ated motion is more diverse hence better encompasses the distribution of real human motion. Secondly, it becomes more likely to generate object-aware motion, making the scene more harmonious and realistic.

Another noteworthy aspect of MobileH2R-Sim is the strategy we adopted to integrate human motion with hand-object poses as shown in figure 6. Building on the already obtained SMPL body model parameters from the motion process, we further utilize the SMPL-X model, which supports both body and hand modeling. We integrate hand poses derived from DexGraspNet, based on the MANO model, into the SMPL-X framework. Additionally, by calculating the mapping relationship between the hand joints of the MANO and SMPL-X models, we obtain a transformation matrix that aligns the hand with the body. This transformation allows the object pose to be projected into the relative pose within the body coordinate system.

For the arm motion during the handover phase, we implemented an optimizer based on joint constraints and task priors as shown in figure 7. Joint constraints include restrictions such as the elbow not bending backward and preventing body or arm mesh interpenetration. Task priors primarily ensure that the distribution of the final handover target points aligns with the task expectations. After obtaining the joint parameters for the arm’s final frame through the optimizer, we generate the arm’s lifting motion by applying appropriate interpolation. Similarly, we add the hand-object pair into this phase following the same scheme as discussed above.

After separately generating full-body motion and arm motion, we designed an effective interacting mechanism for switching between these two phases within the simulation environment. Initially, the human in the simulation only performs full-body motion. The transition from full-body to arm motion is triggered under one of the following conditions: (1) Proximity to the robot: When the distance between the robot and the human falls below a set threshold (0.5m), it is assumed that the human notices the robot’s request to hand over an object. After a reaction time (approximately 200ms on average), the human begins executing the arm motion to hand over the object. (2) Completion of full-body motion: If the full-body motion has been completed (lasting a total of 6 seconds), the human will directly begin executing the arm motion to hand over the object. When both the full-body and arm motions are completed, or when the robot touches the object, the human stops moving and waits for the task to terminate. To address the uncertainty of when the arm motion will be triggered and to avoid the computational burden of real-time calculations, we precompute and cache arm motion at small intervals for each segment of full-body motion. When the arm motion is triggered, the simulation directly uses the cached arm motion for the subsequent time frame.

## A.2. Demonstration Workflow

In our manuscript, we primarily focus on the design of loss functions for demonstration generation to ensure safety and imitation-friendliness. Here, we detail the overall demonstration workflow, with particular attention to overlooked components such as the forecasting window, grasp selection, and stopping distance.

### A.2.1. Step 1: Initialization

Before starting the demonstration, we randomize the scene by applying a global translation and rotation to the human, hand, and object. This randomization serves as a form of data augmentation to enhance model generalization.

### A.2.2. Step 2: Plan Evaluation

We set a predefined **replan interval**. Replanning is triggered under three conditions:

1. The trajectory buffer is empty.
2. The replan interval elapses.
3. Reactive behavior occurs (e.g., transitioning from the pre-handover phase to the handover phase).

If replanning is required, proceed to Step 3; otherwise, execute the current trajectory in Step 4. In our experiments, we set the replan interval to 1.5 seconds. This interval represents a tradeoff:

- **Frequent replanning** slows down demonstration generation due to the computational overhead of replanning (Step 3) and may lead to trajectory discontinuities.
- **Infrequent replanning** risks mimicking GenH2R’s [49] destination planning, which significantly reduces success rates.

### A.2.3. Step 3: Replanning

During each replanning step, the planner uses oracle information from a defined foresee time window to predict the future states of the human, hand, and object. The planner then computes a new trajectory. **Foresee time** plays a crucial role in planner performance, as it determines the planner’s predictive capability. A shorter foresee time resembles dense planning, while a longer one approximates destination planning. Based on empirical testing, we fixed the foresee time to 1.5 seconds, ensuring consistent results across experiments. Replanning involves two substeps:

**Step 3.1** Generating the full-body robot grasping pose.

**Step 3.2** Optimizing the trajectory.

#### Step 3.1: Full-Body Robot Grasping Pose Generation

A naive approach would randomly select a grasping pose for the object, solve for an IK solution using the robot’s URDF, and obtain a final grasping pose. However, this approach often results in collisions with the human or occlusions in the robot’s view.

Instead, we preprocess grasping poses offline (provided by *Acronym* [12]) and rank them in descending order of distance from the human hand. The assumption is that a grasp-

ing pose farther from the human hand will generate a safer full-body pose when the robot is facing the human. Experimental results confirm this assumption.

We further constrain the robot’s base position to a **sector-shaped area** directly facing the human, approximately 0.5–0.8 meters away. Instead of solving these constraints directly, we sample base positions and orientations within the sector. Once the base’s 3 degrees of freedom (DoF) are determined, we attempt to solve IK using the ranked grasping poses. If an IK solution is found, it becomes the final full-body robot pose.

To accelerate this process, we prefilter grasping poses that collide with the human hand. This two-loop approach (outer loop for base sampling, inner loop for grasping pose selection) efficiently finds feasible solutions, as most valid poses are already facing the human.

**Step 3.2: Trajectory Optimization** Given the initial and final grasping poses, we optimize the trajectory using the manuscript-defined obstacle loss and neural loss to ensure safety and distillation-friendliness.

- The **neural loss** incorporates outputs from both the pose prediction network  $P$  and the vision-state recovery estimator  $E$ , both implemented as simple 2-layer MLPs to maintain computational efficiency.
- Training  $E$  requires inputs in both the **end-effector frame** and **robot base frame**, including the human skeleton’s keypoints, human pose, hand pose, and object pose. Since the trajectory is differentiable, gradients propagate through  $E$  to facilitate trajectory optimization.

### A.2.4. Step 4: Trajectory Execution

The robot executes the optimized trajectory. If the trajectory is empty (e.g., due to IK failure), the robot remains stationary to ensure safety.

**Experimental Environment and Data Generation** In our experiments, we utilized the PyBullet environment with Ray for multi-threading. Using an 8-GPU setup (Nvidia GeForce RTX 3090), we achieved a trajectory generation speed of approximately 1 second per trajectory. This setup ensures a success rate of over **80%**, allowing us to efficiently generate a large dataset.

We selected the majority of successful trajectories to serve as training data for subsequent imitation tasks. This approach enabled us to balance speed and accuracy while maintaining high-quality demonstrations.

## A.3. Imitation for coordinated Based-Arm Actions

Our imitation network employs three loss functions:  $\mathcal{L}_{\text{base}}$ ,  $\mathcal{L}_{\text{arm}}$ , and  $\mathcal{L}_{\text{pred}}$ .

- Base Loss ( $\mathcal{L}_{\text{base}}$ ): This loss supervises the robot base’s three degrees of freedom using the L1 loss function.

- Arm Loss ( $\mathcal{L}_{\text{arm}}$ ): Following the approach defined in [25], we use the predicted 6D pose to compute the co-

ordinates of keypoints. The loss is then defined as the difference between the predicted and ground truth keypoint coordinates.

- Prediction Loss ( $\mathcal{L}_{\text{pred}}$ ): Similarly,  $\mathcal{L}_{\text{pred}}$  is defined using the difference between predicted and ground truth keypoint coordinates, following the same procedure as  $\mathcal{L}_{\text{arm}}$ .

At each time step, we retrieve the point clouds from several previous time steps and apply the Iterative Closest Point (ICP) registration algorithm [43] to estimate the transformation matrices between the current point cloud and past point clouds in the world frame.

While these transformations may introduce slight inaccuracies due to the incomplete nature of the point cloud inputs, they still provide sufficient flow information for each point. The estimated flow is then transformed back to the current egocentric frame, forming a crucial component of our feature representation.

In our experiments, we set the weighting coefficients as  $\lambda_1 = \lambda_2 = 1$  and  $\lambda_3 = 0.5$  and set the flow number as 3.

## B. Simulation Experiments Details

### B.1. Training Details

All data generation, training, and evaluation are conducted on an 8-GPU setup with NVIDIA GeForce RTX 3090 GPUs, which ensures high computational efficiency. This setup is user-friendly and widely accessible for researchers with moderate hardware resources. For training, we use a batch size of 512, a learning rate of 0.003, and a weight decay of  $1 \times 10^{-5}$ .

### B.2. Experimental Data Details

#### B.2.1. Evaluation on Different Training Scenes

In the manuscript, we discuss that using the unscalable mocap dataset “s0” results in a significant average drop in the success rate by 34.6%. When trained on the simpler human-involved “m0” dataset, the policy performs well on the simple testing set, with small drops in success rates of 1.8% and 1.4% for “m0” and “s0”, respectively. However, in more complex scenarios, the success rate decreases by 8.1%. This demonstrates that the complexity and diversity of human assets are crucial for the policy’s ability to handle more challenging tasks.

To provide further insights beyond success rates, we list the detailed failure rates in Table 6, categorized into human contact, object drop, and timeout. Among these, **human contact failures** are the most critical to avoid, as collisions with humans can lead to unsafe outcomes. When training on the simpler mocap dataset “s0” compared to “n0”, the drop rate increases by 17.4%, 31.0%, and 19.4% across the three test datasets. Furthermore, when analyzing the absolute number of object drops, training on “s0” results in

increases by factors of 3.63, 2.51, and 4.46 compared to training on “n0”.

These results indicate that solely relying on unscalable real-world data not only decreases success rates but also significantly amplifies the number of object drops, making the resulting policy highly unreliable. This highlights one of our key insights: relying on a large volume of high-quality simulated data can outperform using a small amount of real-world data. For many HRI tasks, such as handover, the lack of specific task datasets is a major challenge. Therefore, rapidly synthesizing high-quality, large-scale simulated datasets is a promising solution.

Similarly, we observe that training on “n0” achieves higher success rates and a lower human contact rate compared to training on “m0”.

It is important to note that these metrics are interrelated. For instance, training on “s0” often results in the highest timeout rate, as the policy struggles to capture the dynamics of the environment and fails to keep up with human actions. This, in turn, leads to a lower probability of human contact or object drops, as human contact requires approaching the human, and object drops require grasping the object. However, even under these circumstances, the human contact rate for “s0” remains the highest among the datasets, underscoring its limitations. This observation further highlights the challenges of training on unscalable real-world data and emphasizes the need for diverse, high-quality simulated data to improve the policy’s generalizability and safety.

#### B.2.2. Evaluation on Different Demonstration Safety Concerns

In the manuscript, we mention that without future obstacle avoidance, the policy’s success rate decreases by an average of 4.0%, and the human contact rate increases from 10.9% to 16.1%. Without final pose constraints, the success rate decreases by an average of 8.0%, and the contact rate rises to 19.8%. These results highlight that demonstrations with a simple safety design can significantly reduce human collisions, which are the most critical failures to avoid compared to object drops or timeouts.

As detailed in Table 7, if we analyze the absolute values, we observe that without future obstacle avoidance, human contact increases by approximately one-third, while without final pose constraints, it doubles. These findings further demonstrate the importance of incorporating these safety designs into the demonstrations.

It is worth noting that we do not discuss **time** or **average success** rates in detail, as these metrics remain largely unaffected across different training assets or demonstration strategies. Average success directly correlates with success rate changes, so our focus remains on **success rates** and **human contact rates**, which provide more meaningful insights into the policy’s performance and safety.

	m0		n0		s0	
	Success	Contact / Drop / Timeout	Success	Contact / Drop / Timeout	Success	Contact / Drop / Timeout
trained on s0	35.3	24.0 / 17.4 / 23.3	22.0	51.5 / 9.9 / 16.6	34.0	25.0 / 11.1 / 29.9
trained on m0	62.0	7.3 / 18.8 / 11.9	45.3	26.8 / 16.3 / 11.6	76.4	9.0 / 9.7 / 4.9
trained on n0	63.8	6.6 / 13.5 / 16.1	53.4	20.5 / 14.1 / 12.0	77.8	5.6 / 10.4 / 6.2

Table 6. **Evaluation on different training scenes.** We train our method on three training sets and evaluate it across three test sets: the relatively simple human-involved scenario ("m0"), complex scenarios ("n0"), and real mocap data ("s0"). "Contact" means human contact, "Drop" means object drop.

	m0		n0		s0	
	Success	Contact / Drop / Timeout	Success	Contact / Drop / Timeout	Success	Contact / Drop / Timeout
w/o FOA	58.7	9.0 / 16.5 / 15.8	48.5	26.9 / 13.6 / 11.0	75.7	10.5 / 6.9 / 6.9
w/o FPC	58.4	13.7 / 20.9 / 7.0	43.2	31.0 / 17.6 / 8.2	69.4	14.6 / 9.7 / 6.3
Ours	63.8	6.6 / 13.5 / 16.1	53.4	20.5 / 14.1 / 12.0	77.8	5.6 / 10.4 / 6.2

Table 7. **Evaluation of different demonstration generation strategies.** We train various methods on "n0" and evaluate them across three test sets: the relatively simple human-involved scenario ("m0"), complex scenarios ("n0"), and real mocap data ("s0"). "FOA" refers to without future obstacle avoidance, and "FPC" refers to without final pose constraints.

### B.3. Discussion on Different Action Types

In the manuscript, we mention that the model learns 6D control actions (3D translation and 3D rotation) for the robot gripper and 3D control actions (2D translation and 1D rotation) for the base. For the base movement, there is no ambiguity—it corresponds to the egocentric SE(2) transformation of the base. However, for the robotic arm, its motion can be decomposed into the base’s movement and the arm’s joint positions. Once the base’s motion is determined, the 6D action output by the policy is used to solve the inverse kinematics (IK) for the arm’s joint angles.

In all our experiments, the 6D action output by the policy represents only the robotic arm’s egocentric action and does not explicitly account for the base’s movement. This approach inherently incorporates the base’s motion into the action representation. During IK computation, we first calculate the base’s future position based on the base action and then compute the arm’s joint positions relative to this future position. The advantage of this approach is that the policy does not need to learn the complex relative motion relationship between the base and the arm.

In contrast, when we attempted to learn the robotic arm’s motion relative to the base, the loss during training appeared normal, but the policy failed to infer reasonable actions. This demonstrates that learning the relative motion relationship is highly challenging. We also experimented with incorporating the relative position between the arm’s end effector and the base as part of the policy’s input, but this approach proved ineffective. Moreover, this method lacks robustness, as the relative relationship between the base and the arm can vary significantly with different robot models, making zero-cost transfer across robots impractical.

Methods	m0	n0	s0
w/o flow	58.0	47.2	53.5
w/o human	51.3	48.7	57.6
w/o coordinated action	51.0	41.7	48.9
deferred feature fusion	55.4	47.8	75.0
only head camera	50.3	43.4	50.7
only wrist camera	43.6	38.7	41.7
Ours	<b>63.8</b>	<b>53.4</b>	<b>77.8</b>

Table 8. **Ablations on different policy designs.** We conduct more ablations on various modules, including different fusion strategies and different perception input.

### B.4. More ablations

We provide additional ablations in Table 8. In the manuscript, we mention that when decoding the arm and base actions separately using two independent networks (e.g., two PointNet++), we observe a dramatic 17.8% decrease in success rate. This demonstrates the necessity of decoding both actions simultaneously. Furthermore, when using two PointNet++ encoders, concatenating their output global features, and decoding the arm and base actions based on this deferred feature fusion strategy, we observe decreases in success rates of 8.4%, 5.6%, and 2.8% across the test scenarios. These results indicate that performing fusion within the set abstraction layers is a more effective strategy for scene fusion, highlighting the importance of early integration of object and human features in the policy network.

In our experiments, we utilized two cameras to mitigate occlusion issues and improve visual perception. To validate the importance of using multiple cameras, we conducted experiments with a single camera setup. When only the head camera is used, the arm frequently occludes the head



camera’s field of view, resulting in success rate decreases of 13.5%, 10%, and 27.1% across the test scenarios. Conversely, when only the wrist camera is used, there are more instances where objects are not visible (e.g., when the robot raises its arm or the view is obstructed by the robot’s body), leading to success rate drops of 20.2%, 14.7%, and 36.1%. These results highlight the importance of multiple cameras in ensuring robust visual perception. In a visual policy, it is critical to provide the policy with as much visual input as possible and effectively fuse the information from multiple sources.

## C. Real World Experiments Details

### C.1. Setup

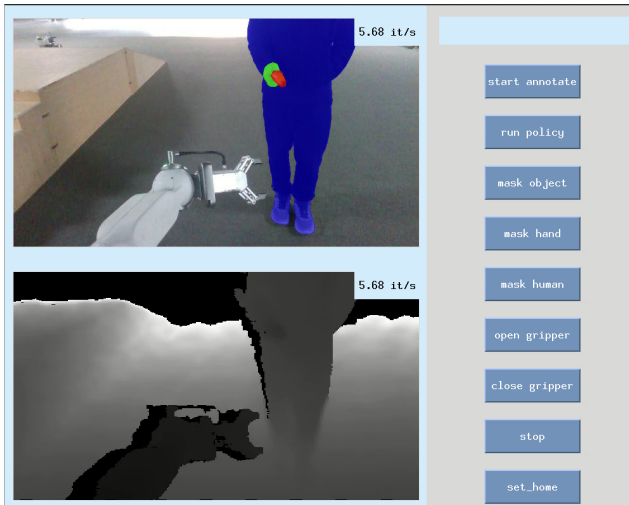


Figure 8. **Our control panel for real-world experiments.** Powered by SAM2, we can accurately track humans and objects and perform rapid segmentation (6-8 FPS). This enables efficient and precise perception, which is crucial for real-time robotic applications.

Since our policy relies on segmented point clouds of the object, the human hand, and the human body, we use SAM2 [41] to obtain segmentation masks in our real-world experiments.

Specifically, we manually annotate the object, the human hand, and the human body in the first RGB image using our control panel as shown in Figure 8, and then leverage the tracking capability of the SAM2 model to generate segmentation masks in the following RGB images. Combining the segmentation masks and the depth map from the depth camera, we obtain the segmented point clouds to be fed into our policy. After annotating the first RGB image, no further human operation is needed until the end of the experiment.

All of the models used in real-world experiments (including the SAM2 model and our policy model) run on a



Figure 9. **Various objects for real-world handover.** The image above displays various objects for mobile handover, including the can, the bowl, the bottles or some plastic objects.

single NVIDIA GeForce RTX 4090 GPU.

We also provide a **supplementary video** that showcases extensive real-world demonstrations of our method. The video includes examples from various scenarios, such as healthcare settings and home office environments. It highlights the generalization of our approach across different human heights, diverse objects, and varying obstacle configurations. Additionally, it demonstrates the safety aspects of our method.

### C.2. User Study

Table 9 provides a detailed breakdown of the results presented in Table 1 of the manuscript. We compare our method with GenH2R(reprod.) across 6 objects in 2 different settings. In the simple setting, users directly hand over the object to mimic “m0”. In the complex setting, users may sit, go downstairs, or perform adversarial actions to mimic “n0”. Our method is compared with baselines across different settings, revealing a remarkable 40% improvement in the simple setting and a substantial 33% improvement in

	Simple setting		Complex setting	
	GenH2R[49]	Ours	GenH2R[49]	Ours
1. mini cocoa crisps	2 / 5	5 / 5	2 / 5	3 / 5
2. adhesive tape	3 / 5	4 / 5	2 / 5	3 / 5
3. chewing gum container	1 / 5	3 / 5	1 / 5	3 / 5
4. instant noodles	1 / 5	4 / 5	1 / 5	4 / 5
5. chicken jerky	3 / 5	4 / 5	1 / 5	4 / 5
6. bottled iced tea	2 / 5	4 / 5	2 / 5	2 / 5
total	12 / 30 (40%)	<b>24 / 30 (80%)</b>	9 / 30 (30%)	<b>19 / 30 (63%)</b>

Table 9. **User study for sim-to-real experiments.** our method and GenH2R(reprod.) method were evaluated by five individuals for six objects in both the simple and complex settings. Failure scenarios included collisions with the human body, dropping on the ground, or exceeding the time limit ( $T_{\max} = 25$  seconds). Our method consistently outperformed the baseline in the real-world handover system in both simple and complex settings, aligning with the results observed in the simulation experiments.

the complex setting from GenH2R.

## D. Limitations and Future Work

While this paper demonstrates significant progress in the human-to-mobile-robot handover task, we acknowledge certain limitations that could inspire exciting future research directions.

**Mobile Robot Considerations.** In this work, we utilized the Galbot robot, which features a 3-DoF omnidirectional base and a 7-DoF robotic arm. Our policy primarily leverages coordinated base-arm actions. However, with the rapid development of humanoid robots, including bipedal robots and various advanced platforms, different application scenarios may require customized measures to improve policy training, such as modifications to the network architecture. Nevertheless, we believe that our scalable pipeline for generating diverse human motions and the automatic, safe, and imitation-friendly demonstration generation process are broadly applicable. Many of the plug-and-play modules used in our approach can be replaced or adjusted to account for the unique characteristics of other robot types, allowing for the design of tailored policies. We look forward to future work extending mobile handover tasks to a wider variety of mobile robots.

**Baseline Comparisons.** We compared our method with non-end-to-end approaches as well as the state-of-the-art method, GenH2R. According to GenH2R’s results, imitation learning significantly outperforms reinforcement learning in simple fixed-based handover tasks. However, in our work, the scenarios are more complex, requiring greater safety considerations, which are challenging to achieve with RL-based methods. As a result, we did not reproduce RL methods in this setting. Of course, there are many potential solutions for mobile human-to-mobile-robot handover tasks, and we hope future frameworks will enable broader comparisons.

**Real-World Deployment.** Our model outputs delta positions, which require robust position control algorithms.

Recent advancements in learning velocity or force control present promising directions that our current framework does not yet consider. Additionally, we observed certain challenges during real-world deployment, such as occasional segmentation errors with SAM2 or inaccuracies in depth camera perception. These anomalies pose significant challenges to our model. To address these issues, incorporating random perturbations during training or fine-tuning the model in real-world settings could improve robustness. Some hybrid methods, such as combining synthetic and real-world data for training, could also be effective. While we achieved excellent results using solely synthetic data, we believe further exploration of these methods will enhance sim2real transfer in the future.